Available online at www.sciencedirect.com

SciVerse ScienceDirect

Structural Integrity Procedia 00 (2016) 000–000

Structural Integrity Procedia

www.elsevier.com/locate/procedia

21st European Conference on Fracture, ECF21, 20-24 June 2016, Catania, Italy

# Interface instabilities of growing hydrides

Per Ståhle*, Wureguli Reheman

*Div. of Solid Mechanics, Lund Institute of Technology, Lund, Sweden*

**Abstract**

Formation of metal hydrides is a serious complication that occur when hydride forming metals such as Zirkonium, Niobium, Vanadium and Magnesium are exposed to long term hydrogen environment. The main concern is that the hydride, as being a brittle material, has very poor fracture mechanical properties. Formation of hydride is associated with transportion of hydrogen along the gradients of increasing hydrostatic stress, which leads to crack tips and other stress concentrators, where it forms the hydride. In the present study the themodynamics of the evolving hydrides is studied. The focus is on the evolution of the interface between the metal and the evolving hydride. The process is driven by the release of free strain, chemical, and gradient energies. A phase field model is used to capture the driving forces that the release of the free energy causes. The study gives the conditions that lead to hydride advancement versus retreat and under which conditions the metal-hydride interface becomes unstable and develops a waviness. The spatial frequency spectrum leading to instability is found to depend on the ratio of the elastic strain energy density and parameters related to the interface energy. The theory is related to the Asaro-Tiller-Grinfeld theory for surface instabilities.

Peer-review under responsibility of the Scientific Committee of ECF21.

*Keywords:* Metal hydride; Growth; Platelets

## 1. Introduction

When structural materials are exposed to a long term hydrogen environment they may interact with hydrogen, and cause various kinds of structural damages due to metal degradation. The interaction and damage of hydrogen depend on a range of conditions. In the metals that form hydride, the precipitation of small and local amounts of hydrides strongly affect the local mechanical properties and the over all integrity of the entire structure.

With the increasing need for green energy, hydrogen fuel cell technologies are used as renewable energy resources. As a consequence secure vessels for transport and storage of liquid hydrogen is required. Much of the efforts are done to the selection and production of secure transportation and storage materials. However, the effect of the hydrogen to the transportation vessels are unavoidably associated with interaction between the hydrogen and the base material. In nuclear power production metallic zirconium is exposed to hydrogen as it used extensively as structural support for the fuel and the control rods. Zirconium forms brittle hydrides in hydrogen environments, which may case serious prob-

* Per Ståhle. Tel.: +46-70-553-9492
*E-mail address:* per.stahle@solid.lth.se


Peer-review under responsibility of the Scientific Committee of ECF21.

lems. Other hydride forming metals of practical interest include magnesium, titanium, hafnium. In many applications of these metals, the formation of hydride is considered to be a major life limiting factor.

When the hydrogen concentration is sufficient, it reacts with the metal and forms a metal hydride. The hydride is a binary brittle compound, which generally has a very low strength (see, Troiano (1960), Ellyin and Wu (1994), Viswanathan et al. (2006)). Hydrogen migrates along gradients of hydrostatic stress and accumulates where the stress obtains a local maximum (see, e.g., Singh et al. (2005)). The hydrogen, therefore, accumulates at material defects, crack tips, dislocation pile-ups and other stress concentrators. The reason for the attraction of the hydrogen along the gradient of hydrostatic stress is that the metal expands with increasing hydrogen concentration, which releases energy caused by the relaxation of the hydrostatic stress. As an example, the stress free volumetric expansion of zirconium during hydridisation can be of the order of 15 to 20%.

The hydride formation is a complicated process that results from the simultaneous operation of several coupled processes. There is an agreement that the hydride is formed when the hydrogen concentration exceeds its terminal solid solubility of the material, provided that a few additional conditions are fulfilled. When the hydride reaches a certain size, it cracks at a comparably small load. A new hydride is after that, reformed ahead of the extended crack. The result is an incremental type of crack growth Singh et al. (2008). A complete understanding involves several disciplines such as atomic physics, electro-chemistry, materials engineering, and fracture mechanics. Many experimental and theoretical studies have had focus on the hydride formation at crack tips and its influence on the strength of the material (Nuttall et al. (1976)). Models of crack propagation based on the effect of diffusion was studied by Shi (1999), Svoboda and Fischer (2012) and models that studied the importance of threshold hydrogen concentration was studied by Singh et al. (2005). Temperature changes and hydrogen content related models have been investigated by Bertolino et al. (2003).

The mechanical stress play a key role, not only for the transportation of the hydrogen into the vicinity of the crack tip, but also for the morphology of the growing hydrides. Further, the hydrides appear different on different length scales, i.e. on a mm length scale and above it may appear as a solid hydride, on a finer scale between of the order of tens of microns appear as fractioned into so called platelets.

The morphological and microstructural differences of hydride precipitates affect the fracture process and has consequences for the strength of the material. A phase field model that includes mechanical, interface and gradient energies, allows us to compute the thermodynamics of the process. In the present study the evolution of the morphology of the metal to hydride interface is examined regarding growth, retraction and interface stability.

In Sect. 2 the theory is developed and governing partial differential equations are given for the distribution of the phase and the deformation components. In Sect. 3 the phase distribution in the interface region is derived for a few simplified cases. Both planar and wavy interfaces are included. In Sect. 4 numerical solutions are first established by comparative studies of the simplified cases. Here also, the limits for numerical accuracy is set.

## 2. Phase Field Modelling

For a virtually sharp interface, treated as a discontinuity, specific chemical and mechanical properties may be ascribed to the interface. This simplifies the analysis and normally has no significant influence on the thermodynamical behaviour of the body. However, when the distance between structural inhomogeneities or other characteristic distances are of the same order of magnitude as the thickness of the interface, e.g., at a rough interface, at the tip of a crack or during emission of dislocations, etc., the thickness of the interface may play a role and the negligence thereof may lead to unrealistic predictions. As opposed to this, a diffuse interface model assumes a continuous variation of composition, structure and other properties within the modelled region (cf. Landau and Lifshitz (1935)). This includes both the hydride and the metallic matrix material and the diffuse interface between them.

Here, the solid material is assumed to be linear elastic with the elastic modulus $E$ and Poisson's ratio $\nu$. The energy of the system is composed of the Landau chemical potential energy, the gradient energy and the elastic energy. The respective energy densities are $F_{ch}$, $F_{gr}$, and $F_{el}$. The total free energy is defined as an integral that covering the complete system. In the formulated system the essential free energies are assumed to be chemical, gradient and strain energies. In the total energy is assumed to be

$$\mathcal{F} = \int_V (F_{ch} + F_{gr} + F_{el}) \mathrm{d}V \,, \tag{1}$$

where $V$ is the volume of the body. The chemical, gradient and elastic energy densities are defined as follows,

$$F_{ch} = p(\frac{1}{4}\psi^4 - \frac{1}{2}\psi^2), \quad F_{gr} = \frac{g_b}{2}\psi_{,i}\psi_{,i} \quad \text{and} \quad F_{el} = \frac{1}{2}\sigma_{ij}(\psi)\epsilon_{ij}\,. \tag{2}$$

Here $\psi$ is a phase variable that keep track of the phase. The permissible interval is $-1 \le \psi \le 1$, in which $\psi = -1$ defines the original material and $\psi = 1$ defines the precipitate. All material properties are in general functions of $\psi$. The summation rule is applied for double indices and the notation $(\,)_{,i} = \partial(\,)/\partial x_i$ is used.

$F_{ch}$ is the Landau chemical potential energy density that represents the free energies stored in the different phases. The energy density is caused by the disorder that arise in mixed phases. When $F_{ch}$ play a significant role, the boy is split up into two phases defined as regions consisting of almost pure original material and pure precipitate. These regions are then separated by a thin layer called the interface consisting of an unpure material. The width of the interface is denoted $b$ and is in this study defined as the region in which $\psi \le 0.9$.

$F_{gr}$ is an energy density that is caused by a Brownian motion that counteracts concentration gradients. Finally, $F_{el}$ is the elastic strain energy density for materials with a traction free expansion strain $\epsilon_s(\psi)$.

The theory is based on the Ginzburg-Landau's assumption that the evolution in any point of any state variable depends on the release rate of the local free energy density with respect to a variation of that variable. In the present case with $F = F_{ch} + F_{gr} + F_{el}$, the Ginzburg-Landau assumtion is formulated,

$$\frac{\partial(\,)}{\partial t} = -L_{()}\frac{\delta F}{\delta(\,)}, \tag{3}$$

In the present study $(\,)$ represents the phase variable $\psi$ or the displacements $u_i$.

According to Lagranian formalism the following relate the variation to partial derivatives of $F$ with respect to scalar variables $(\,)$ and its spatial derivatives $(\,)_{,i}$ as follows,

$$\frac{\delta F}{\delta(\,)} = \frac{\partial F}{\partial(\,)} - \frac{\partial}{\partial x_i}\frac{\partial F}{\partial(\,)_{,i}}. \tag{4}$$

The notation for spatial derivatives is used for indices $i$, $j$ and $k$. The variations with respect to $\delta\psi$ are readily obtained for the chemical and gradient energy densities as

$$\frac{\delta F_{ch}}{\delta\psi} = -p(1-\psi^2)\psi \quad \text{and} \quad \frac{\delta F_{gr}}{\delta\psi} = -g_b\psi_{,ii}. \tag{5}$$

Further, stresses are given by

$$\sigma_{ij}(\psi, u_i) = 2\mu\epsilon^e_{ij}(\psi, u_i) + \lambda\delta_{ij}\epsilon^e_{kk}(\psi, u_i)\,, \tag{6}$$

where $\mu$ and $\lambda$ are the Lamé parameters and $\delta_{ij}$ is the Kronecker delta. The total strain $\epsilon_{ij}$ is defined as follows,

$$\epsilon_{ij}(u_i) = \frac{1}{2}(u_{i,j} + u_{i,j})\,. \tag{7}$$

where $\epsilon^e_{ij}$ is the elastic strain, defined as

$$\epsilon^e_{ij}(\psi, u_i) = \epsilon_{ij}(u_i) - \delta_{ij}\epsilon_s(\psi, u_i)\,, \tag{8}$$

The stress free linear expansion, $\epsilon_s(\psi)$, is chosen to be 0 for $\psi = -1$ and $\epsilon_v/3$ for $\psi = 1$, where $\epsilon_v$ is the volumetric stress free expansion. Further, it is necessary that $\epsilon'_s(\psi) = 0$ at $|\psi| = 1$ to avoid discontinuous behaviour at the edges of the permissible interval for $\psi$. The simplest polynomial that fulfils the conditions is

$$\epsilon_s(\psi) = -\frac{1}{12}(\psi^3 - 3\psi - 2)\epsilon_v. \tag{9}$$

Insertion of Eqs. (6) and (8) into (2) gives the following expression

$$F_{el} = \int_0^{\epsilon_{ij}} \sigma_{ij}\, \mathrm{d}\epsilon_{ij} = \int_0^{\epsilon_{ij}} \sigma_{ij}\, \mathrm{d}\epsilon^e_{ij} + \int_0^{\epsilon_{ij}} \sigma_{ij}\, \mathrm{d}\epsilon_s = \frac{1}{2}\sigma_{ij}\epsilon^e_{ij} + \sigma_{ii}\epsilon_s. \tag{10}$$

Application of (4) and (9) gives on,

$$\frac{\delta F_{el}}{\delta \psi} = \frac{1}{4}\sigma_{ii}(1-\psi^2)\epsilon_v, \tag{11}$$

Application of (3) on the results (5) and (11) gives the governing equation for the evolution of $\psi$ as follows

$$\frac{\partial \psi}{\partial t} = L_\psi \left( p(1-\psi^2)\psi + g_b\psi_{,ii} + \frac{1}{4}\sigma_{ii}(1-\psi^2)\epsilon_v \right), \tag{12}$$

Regarding the displacements, $u_i$, the governing equation can be found as following with the same formalism as for the phase variable. Obviously

$$\frac{\delta F_{ch}}{\delta u_i} = \frac{\delta F_{gr}}{\delta u_i} = 0\,. \tag{13}$$

Using (4) and (7) one obtains

$$\frac{\delta F_{el}}{\delta u_i} = -\frac{\partial}{\partial x_j}\frac{\partial F_{el}}{\partial (u_{i,j})} = -\frac{1}{2}\{2\mu\epsilon_{ij,j} + \lambda\epsilon_{jj,i}\} - (3\lambda+2\mu)\epsilon_s(\psi)_{,i}\,. \tag{14}$$

In the present study only quasi-static evolution is considered. The body may be in a thermodynamic state but the mechanical state is assumed to be static. By putting the mobility parameter $L_{u_i} \gg \partial u_i/\partial t$ implying that,

$$\frac{\delta F_{el}}{\delta u_i} = 0 \;\Rightarrow\; 2\mu\epsilon_{ij,j} + \lambda\epsilon_{jj,i} - 2(3\lambda+2\mu)\epsilon_s(\psi)_{,i} = 0\,. \tag{15}$$

The governing equation for the evolution of the displacements, $u_i$, is as follows

$$u_{i,jj} + \frac{1}{1-2\nu}u_{j,ji} = \frac{1+\nu}{1-2\nu}\epsilon_v(1-\psi^2)\psi_{,i}\,, \tag{16}$$

which is identical to $\sigma_{ij,j} = 0$ for a material with an isotropic stress free volumetric expansion $\epsilon_v$.

With the length unit $\sqrt{g_b/p}$ and the time unit $(L_\psi p)^{-1}$ used in Eqs. (12) and (16), the governing equations take the form

$$\frac{\partial \psi}{\partial \hat{t}} - \psi_{,\alpha\alpha} = \left(\frac{1}{4}\hat{\epsilon}_v\hat{\sigma}_{\beta\beta} + \psi\right)(1-\psi^2), \tag{17}$$

$$\hat{u}_{\alpha,\beta\beta} + \frac{2(1+\nu)}{1-2\nu}\hat{u}_{\beta,\alpha\beta} = 2\frac{(1+\nu)^2}{1-2\nu}\hat{\epsilon}_v(1-\psi^2)\psi_{,\alpha} \tag{18}$$

where the following scalings are made

$$\hat{t} = L_\psi p\, t, \quad \hat{x}_i = \sqrt{\frac{p}{g_b}}x_i, \quad \hat{u}_i = \sqrt{\frac{E}{g_b}}u_i\,. \tag{19}$$

and consequently

$$\hat{\epsilon}_{\alpha\alpha} = \sqrt{\frac{E}{p}}\epsilon_{ij}, \quad \hat{\epsilon}_v = \sqrt{\frac{E}{p}}\epsilon_v\,, \quad \hat{\sigma}_{\alpha\alpha} = \frac{1}{\sqrt{Ep}}\sigma_{ij}, \quad . \tag{20}$$

The index notation for partial derivatives using greek letters $\alpha$, and $\beta$ denotes that the partial derivatives are taken with respect to the non-dimensional coordinates, e.g. $(\,)_{,\alpha}$ denotes $\partial(\,)/\partial\hat{x}_\alpha$, where $\alpha$=1, 2 or 3.

## 3. Solutions for Plane and Shallow Wavy Interfaces

In the absence of mechanical load an analytical solution is given for a straight edge by Ginzburg and Landau (1950). Closed form solutions that include the effect of an external homogeneous stress field are easily obtained as is shown in the following section.

The modelled geometry is a strip with the dimensions of $|x_1| \le h/2$ and $|x_2| \le 3h/2$, where $h$ is height of the studied geometry. The interface is parallel with the $x_1$ axis. and is initially placed at $x_2 = 0$. In the following subsections constant displacements along the edges at $|x_1| = h/2$, respectively constant stress along the edges at $|x_2| = 3h/2$ are applied. In both cases the applied load creates stress and strain fields that are only dependent on the $x_2$ coordinate and time.

### *3.1. Uniaxial stress field applied in the $x_2$ direction, $\psi = f(\hat{x}_2, \hat{t})$*

Here the solution for an edge moving under steady state conditions in a uniaxial stress field, under plane stress condition, is derived. The boundary conditions are

$$\sigma_{22}(\pm 3h/2) = \sigma_o \quad \text{and} \quad \sigma_{12}(\pm 3h/2) = 0, \tag{21}$$

where the stress $\sigma_o$ is constant. Remaining boundaries are traction free. The phase boundary conditions are

$$f(\pm 3h/2) = \pm 1\,, \tag{22}$$

The notation $\psi = f(\hat{x}_2, \hat{t})$ is used, with $\dot{f} = \partial f/\partial\hat{t}$ and $f' = \partial f/\partial\hat{x}_2$. Equation (17) is written

$$\dot{f} - f'' = (\hat{\epsilon}_v\hat{\sigma}_o/4 + f)\,(1 - f^2), \tag{23}$$

where $\hat{\sigma}_o$ equals $\sigma_o/\sqrt{Ep}$. The variation of the contraction across the edge creates a complicated stress-strain distribution close to where the edges meets the boundaries at $|x_1| = h/2$ and $|x_2| = 3h/2$. The disturbance reside in a region that has the linear extent of around two or three distances equivalent the width of the interface, i.e., only a small fraction of the width of the body. To avoid the disturbance and without loosing generality Poisson's ratio is put to $\nu = 0$.

The assumed steady-state conditions implies that $f(\hat{x}_2, \hat{t}) = g(\hat{x}_2 - c\hat{t}) = g(\xi)$ by the coordinate transformation $\xi = \hat{x}_2 - c\hat{t}$. Thus, $\dot{g} = -cg'(\hat{x}_2 - c\hat{t}) = -cg'(\xi)$, which applied to (23) gives,

$$cg' + g'' = -(\hat{\epsilon}_v\hat{\sigma}_o/4 + g)\,(1 - g^2). \tag{24}$$

By putting $z(\hat{x}) = g'$ and $z'(\hat{x}) = z\frac{\mathrm{d}\hat{x}_2}{\mathrm{d}g}\frac{\mathrm{d}z}{\mathrm{d}\hat{x}_2} = z\frac{\mathrm{d}z}{\mathrm{d}g}$ one obtains,

$$\frac{1}{2}\frac{\mathrm{d}(z^2)}{\mathrm{d}f} = -cz - (\hat{\epsilon}_v\hat{\sigma}_o/4 + f)(1 - f^2). \tag{25}$$

After integrating with respect to $\hat{x}$ one obtains

$$z^2 = -2\int\{cz + \frac{1}{4}\hat{\epsilon}_v\hat{\sigma}_o(1 - g^2)\}\mathrm{d}g - g^2 + \frac{1}{2}g^4 + C, \tag{26}$$

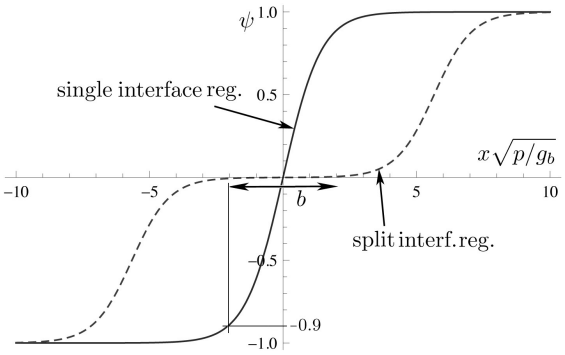


Fig. 1. The phase distribution $\psi$ for a single wave and a split wave that that is caused by large stresses.

The boundary conditions (22) give $C = 1/2$. The roots are found after factorisation of the left hand side as

$$\{z - \frac{1}{\sqrt{2}}(1-g^2)\}\{z + \frac{1}{\sqrt{2}}(1-g^2)\} = -2\int\{cz + \frac{1}{4}\hat{\epsilon}_v\hat{\sigma}_o(1-g^2)\}\mathrm{d}g, \tag{27}$$

Obviously the system has a root $z = -(1/\sqrt{2})(1-g^2)$ if $c$ is chosen to $\sqrt{2}\hat{\epsilon}_v\hat{\sigma}_o/4$ and $z = (1/\sqrt{2})(1-g^2)$ if $c$ is chosen to $-\sqrt{2}\hat{\epsilon}_v\hat{\sigma}_o/4$. The two permissible solutions are

$$\frac{1}{z} = \frac{\mathrm{d}\xi}{\mathrm{d}g} = \pm\sqrt{2}/(1-g^2)\,, \tag{28}$$

with the solution

$$g = \pm\tanh(\frac{\xi}{\sqrt{2}}) = \tanh(\frac{\hat{x}_2}{\sqrt{2}} \mp \frac{\hat{\epsilon}_v\hat{\sigma}_o}{4}\hat{t})\,. \tag{29}$$

The width, $b$, of the interface, i.e., the region where $|g| \le 0.9$, denoted $b_o$ in the present case when $\sigma_{kk} = 0$ along $\xi = 0$, is

$$b_o = 2\sqrt{2}\,\mathrm{arctanh}\,(0.9)\sqrt{\frac{g_b}{p}} = 4.16407\sqrt{\frac{g_b}{p}} \tag{30}$$

The solution shows that the interaction between the interface at around $\xi = 0$ and its surroundings is very small. The deviation from the value it converges to at large distances, i.e. $|g| \to 1$ as $|\xi| \to \infty$ is, e.g., less than one percent for $\xi = 3.75$ and less than $10^{-4}$ for $\xi = 5.4$. It is also obvious that two or more waves can be superimposed as long as the the distance between the waves is large and the boundary conditions are fulfilled.

### *3.2. Uniaxial stress field applied in the $x_1$ direction, $\psi = f(\hat{x}_2, \hat{t})$*

Here a load is applied in the $x_1$ direction via a prescribed displacement

$$u_1(\pm h/2) = \pm\epsilon_o h/2 \quad \text{and} \quad \sigma_{22}(\pm 3h/2) = 0, \tag{31}$$

which gives a stress $\sigma_{11}$ that varies in the $x_2$ direction, i.e.,

$$\sigma_o = (2\mu + 3\lambda)\epsilon^e_{11} = 2\mu\frac{1+\nu}{1-2\nu}\{\epsilon_{11} - 2\epsilon_s(f(\hat{x}_2, \hat{t}))\}. \tag{32}$$

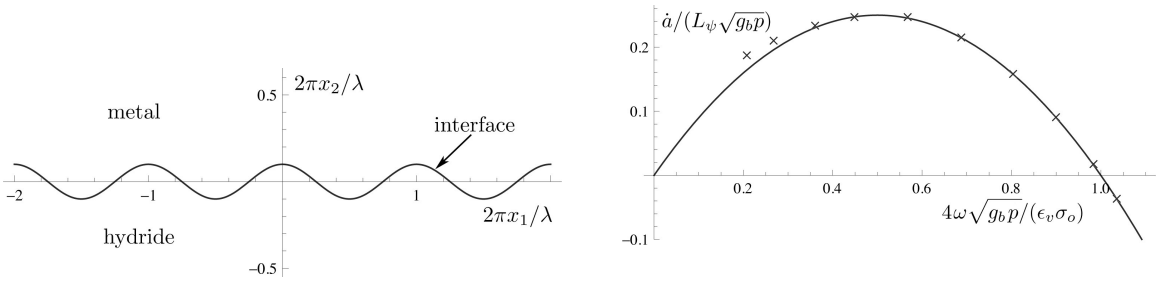


Fig. 2. a) Wavy initial interface with a wavelength $\lambda$ and a wave amplitude $a = 0.1\lambda$. b) Growth rate versus the wave number $\omega = 1/\lambda$.

where the stress $\epsilon_o$ is constant. Remaining boundaries are traction free. Shear traction vanishes on all boundaries. The phase boundary conditions are according to (22).

### *3.3. Wavy interface and subjected to a remote uniaxial stress field applied in the $x_1$ direction*

A wavy interface with a wave amplitude $a$ and the wavelength $\lambda$ is considered. As shown in Fig. 2a the hydride initially occupies the region $x_2 \le a\sin(2\pi x_1/\lambda)$ and the remaining part is the metal. The initial field $g$ is chosen to be

$$\psi = -\tanh\left[\frac{2}{b_o}(x_2 - a\cos(2\pi x_1/\lambda))\right], \tag{33}$$

where $b_o$ is the half thickness of the interface according to (30). Because of the periodicity, the geometry is reduced to one for a strip with the width $0 \le x_1 \le \lambda/2$. The boundary conditions are according to (22) and (31).

The amplitude $a$ is assumed to be small and much less than the wave length $\lambda$. A series expansion for small a gives

$$\psi = -\tanh(2x_2/b_o) + (2a/b_o)\mathrm{sech}(2x_2/b_o)^2\cos(2\pi x_1/\lambda), \tag{34}$$

where $\alpha = \sqrt{2}\arctan(0.9)/b$. Fourier transform of (17) with respect to $x_2$ gives the following relation

$$\frac{\partial\psi}{\partial\hat{t}} = \left(\frac{1}{4}\hat{\epsilon}_v\hat{\sigma}_o - \omega\sqrt{g_b/p}\right)\omega\sqrt{g_b/p}\,\psi, \tag{35}$$

where $\omega = 1/\lambda$ is the wave number (see Fig. 2b).

## 4. Results and Discussion

The finite element code ABAQUS is used to solve the equations (17) and (18). A geometry with the heigth five times the width. Is used. The region is divided into 10000 equal rectangular four node isoparametric finite elements. The number of elements in the width direction, the $x_1$-direction is from 1 for one dimensional cases to 100 for two dimensional cases.

First the problem for a straight edge is studied, i.e. the center of the straight transition region is stationary at $x_1 = 0$. The region is exposed to a constant uniaxial stress perpendicular to the edge, i.e., $\sigma_{11} = 0$ and $\sigma_{22} = \sigma_o$. This leads to a transition region that moves at constant speed in the positive $x_2$-direction for $\sigma_o > 0$. The only relevant physical length is $\sqrt{g_b/p}$. However, the size of the elements and the increment length in relation to the motion rate times the time increment that is being used, introduce undesirable artificial length scales. To avoid the limitations that the artificial dependencies and to examine the accuracy the numerical result for the variation of the phase variable, $\psi$, in the transition region is compared with the corresponding analytical solution.

Figure 3a, shows the result for two different length scales where the one with the larger scale, one with 2 to 3 elements covering the transition region and one with around twice as many elements. Obviously the denser mesh

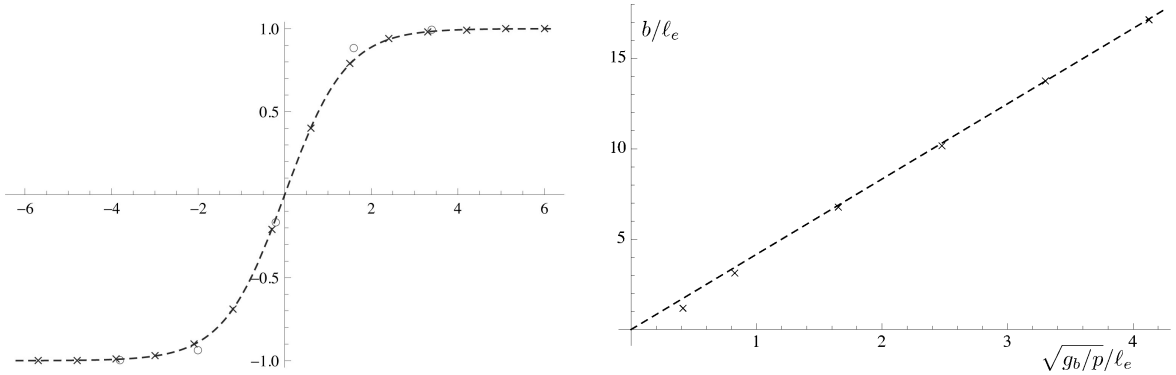


Fig. 3. a) Results for a transition region covered by 2 or 3 finite elements and 7 or 8 elements respectively. b) Number of elements per per calculated width $b_o/\ell_e$ vs. the ratio of the selected interface length scale and the element size $\sqrt{g_b/p}/\ell_e$.

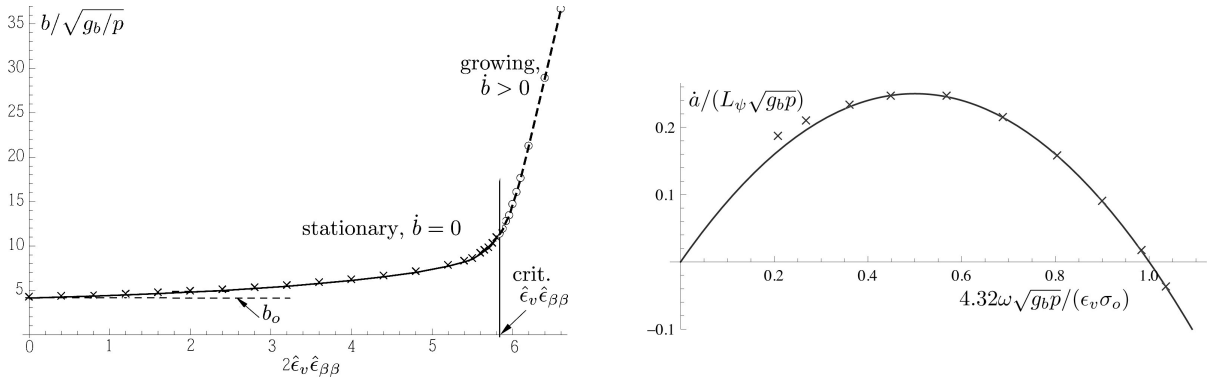


Fig. 4. a) Calculations made for different amounts of straining $\hat{\epsilon}_v\hat{\epsilon}_{\beta\beta}$ from zero to above 6. The critical straining $\hat{\epsilon}_v\hat{\epsilon}_{\beta\beta} \approx 5.8$ marks a switch from stationary width to growing width, seemingly with a constant rate. The curve for $\hat{\epsilon}_v\hat{\epsilon}_{\beta\beta} > 5.8$ depends on time. Here the result for $\hat{t} = 60$ is plotted. b) Growth rate of wave amplitude for a wavy interface. The curve showing the analytical result (35) included.

follow the exact result closely whine the coarser mesh seems to underestimate the width of the transition region with typically 5 to 15%.

The effect of element size on the width of the interface is displayed in Fig. 3b, showing the normalized width $b_o/\ell_e$, where $\ell_e$ is the linear size of the finite elements. The result is displayed as a function of the magnitude of the physical length scale normalised with the element size as $\sqrt{g_b/p}/\ell_e$. The exact result (30) is included in the figure as a dashed line. It is observed that the linear relation between $b$ and $\sqrt{g_b/p}$ is accurate as long as the transition region is large compared with the size of the elements. The numerical result more or less coincides with the exact result as long as the length scale $\sqrt{g_b/p}$ is larger than more than around $1.6\ell_e$. The error is 37%, 12% and 2.7% for $\sqrt{g_b/p}$ equal to 0.4, 0.8 and 1.65 times $\ell_e$ respectively. The same also means that the width of the interface region, $b_o$, is covered by a minimum of around 1, 3 and 7 elements across. In the following calculations the length parameter is set to $\sqrt{g_b/p} \leq \ell_e$ which means that the transition region, $b_o$, is covered by at least four elements across its thickness.

Figure 4a shows the resulting width of the interface for different stretching of along the the interface. The stretching is given on non-dimensional form as $\hat{\epsilon}_v\hat{\epsilon}_{\beta\beta}$. The non dimensional width, $b/\sqrt{g_b/p}$, is stable and increasing with increasing stretching for $2\hat{\epsilon}_v\hat{\epsilon}_{\beta\beta} < 5.8$. For larger stretching the width grows with a seemingly constant speed. Therefore the result for $2\hat{\epsilon}_v\hat{\epsilon}_{\beta\beta} > 5.8$ is time dependent. In Fig. 4a the the result is taken for the non-dimensional time $\hat{t} = 60$. The details around what happens at the critical stretching, $2\hat{\epsilon}_v\hat{\epsilon}_{\beta\beta} = 5.8$, is yet somewhat unclear. The implication is that the hydride would be forming to 50% and homogeneous or complete the formation of hydride in 50% of the volume. The present analysis does not reveal any details regarding this.

The simulations of the wavy surface where initially given an amplitude of a tenth of the wavelength, i.e. $a = 0.1\lambda$. The growth of the amplitude after $\hat{t} = 1$. At the end the relation between the amplitude was in all cases less than the

wavelength. The result displayed in Fig. 4b shows that the simulations rather closely follows the analytical result. Some deviation is observed for the smallest frequencies. For frequencies larger than $\omega > (1/4)\sqrt{g_b/\frac{g_b}{p}}\hat{\epsilon}_v\hat{\sigma}_o$ the interface develops in a stable manner. Initial shapes with a Fourier spectrum with frequencies larger than n $\omega > \frac{1}{4}\sqrt{\frac{g_b}{p}}\hat{\epsilon}_v\hat{\sigma}_o$ will have amplitudes that decay with time.

## 5. Conclusions

It was possible to perform a phase-field analysis of the evolution of a metal to hydride interface. For a plane interface, width and growth rate is obtained analytically. Also a solution for a shallow wavy surface is obtained. The results was reproduced using a finite element method. Very good accuracy was obtained for small loads. For lager loads an unforseen behaviour was observed.

The implications for the fracture process of hydride forming metals are important in the sense that it inform about the different formation processes depending on both stress levels, stress directions and the importance of elapsed time.

*Acknowledgements*

Support from The Swedish Research Council under grant no 2011-5561 is acknowledged.

## References

Bertolino, G., Meyer, G., Perez Ipiña, J., 2003. Effects of hydrogen content and temperature on fracture toughness of zircaloy-4. Journal of Nuclear Materials 320, 272–279.

Ellyin, F., Wu, J., 1994. Effect of hydride precipitation on the elastoplastic stress field near a crack tip. Acta metallurgica et materialia 42, 2709–2717.

Ginzburg, V., Landau, L., 1950. On the theory of superconductivity (in russian). J. Exptl. Theoret. Physo (USSR) 20, 1064.

Landau, L., Lifshitz, E., 1935. Theory of the dispersion of magnetic permeability in ferromagnetic bodies. Phys Zeit Sowjetunion 8, 153.

Nuttall, K., McCooeye, D., Rogowski, A., Havelock, F., 1976. Metallographic observations of the interaction of hydride, stress and crack growth at 600 k in a zr-2.5% nb alloy. Scripta Metallurgica 10, 979–982.

Shi, S.Q., 1999. Diffusion-controlled hydride growth near crack tip in zirconium under temperature transients. Journal of nuclear materials 275, 318–323.

Singh, R., Mukherjee, S., Gupta, A., Banerjee, S., 2005. Terminal solid solubility of hydrogen in zr-alloy pressure tube materials. Journal of alloys and compounds 389, 102–112.

Singh, R., Ståhle, P., Banks-Sills, L., Ristinmaa, M., Banerjee, S., 2008. $\delta$-hydride habit plane determination in $\alpha$-zirconium at 298 k by strain energy minimiz ation technique, in: Defect and Diffusion Forum, Trans Tech Publ. pp. 105–110.

Svoboda, J., Fischer, F., 2012. Modelling for hydrogen diffusion in metals with traps revisited. Acta Materialia 60, 1211–1220.

Troiano, A., 1960. The role of hydrogen and other interstitials in the mechanical behavior of metals. trans. ASM 52, 54–80.

Viswanathan, U., Singh, R., Basak, C., Anantharaman, S., Sahoo, K., 2006. Evaluation of effect of hydrogen on toughness of zircaloy-2 by instrumented drop weight impact testing. Journal of nuclear materials 350, 310–319.